

# ONE-DIMENSIONAL WAVE DISPERSION IN LAYERED MEDIA\*

H. OCKENDON<sup>†</sup>, J. R. OCKENDON<sup>†</sup>, C. L. FARMER<sup>†‡</sup>, AND D. J. ALLWRIGHT<sup>†</sup>

**Abstract.** Homogenisation theory reveals that long one-dimensional waves propagating in a medium with spatially periodic wave speed can behave like dispersive waves in an appropriately homogenised medium. However the precise time and length scales over which this dispersive behaviour is a good approximation are not clear. This paper describes what happens in a specific case when the sound speed and initial conditions allow the problem to be reduced to a finite system of difference equations which can be solved exactly. The long-time asymptotics are compared with the predictions of homogenisation theory and new light is shed on the dispersion phenomenon.

**Key words.** wave propagation, periodic media, multiple scales, homogenization, dispersion

**AMS subject classifications.** 35B27, 34E13, 35L53, 35P25

**1. Introduction.** This paper considers an initial/boundary value problem for one-dimensional wave propagation in which the wave speed varies periodically on a scale much shorter than the propagation distance. Although there is a large literature on such problems, the precise situation that stimulated our research was one in which the wave speed and initial/boundary conditions were sufficiently simple piecewise-constant functions for the problem to be reduced to a finite-dimensional system of difference equations. The importance of such models is that the solution can be found numerically to within rounding errors and hence can be used as a yardstick for assessing the predictions of homogenisation theory, and in particular the long-time effects of wave dispersion.

Systematic homogenisation theory for this type of wave propagation has been pioneered by Santosa and Symes [12], with more recent work done by Abdulle, Grote and Stohrer [1], Yong and Kevorkian [14] and Dohnal, Lamacz and Schweizer [4]. It can be applied to many linear wave equations with spatially periodic coefficients but we will only consider the special (dimensionless) case

$$(1.1) \quad c^2(X) \frac{\partial^2 u}{\partial x^2} = \frac{\partial^2 u}{\partial t^2},$$

where  $c$  is periodic,  $X = x/\epsilon$  with  $\epsilon \ll 1$  and the initial/boundary conditions are independent of  $\epsilon$ . We do however remark that wave propagation in inhomogeneous media is more commonly modelled by rewriting (1.1) as

$$(1.2) \quad \frac{\partial}{\partial x} \left( c^2 \frac{\partial v}{\partial x} \right) = \frac{\partial^2 v}{\partial t^2},$$

and, in one dimension, the two formulations are related by  $v = \partial u / \partial x$ .

As will be recalled in section 2, the principal prediction of homogenisation theory for (1.1) is that, for  $x, t = O(1)$ , averaged wave propagation is at a homogenised speed  $c_H$  which is less than the average speed of a wavefront satisfying  $dx/dt = c$ . Moreover the theory predicts that, for  $x, t = O(\epsilon^{-2})$ , averaged waves propagating at

---

\*This work was partially supported by the Oxford-Martin School Programme on Resource Stewardship and by the Smith Institute.

<sup>†</sup>OCIAM, Mathematical Institute, University of Oxford, Oxford, OX2 6GG, United Kingdom.

<sup>‡</sup>Corresponding author: farmer@maths.ox.ac.uk

the homogenised wave speed are dispersive and can be modelled by introducing a fourth-order spatial derivative into (1.1) or (1.2).

The analysis of our model piecewise-constant problem, described in section 3, sheds new light on the predictions of homogenisation theory. We rely heavily on numerical evaluations of the exact solutions of the model, both in its p.d.e. formulation and its finite-dimensional formulation. Relevant numerical studies have already been carried out by Burrige et al.[3] and by Santosa and Symes[12]. The work of Fogarty and Leveque [6] is of special relevance as they have derived exact ‘characteristic difference’ relations for hyperbolic conservation laws in which the data is piecewise constant. Also we will see that the analysis of an underpinning wave-reflection problem can be done simply in terms of wave momentum.

Finally, in section 4, we consider two explicit representations of the solutions of both the p.d.e. problem and its finite-dimensional equivalent which reveal the dispersive phenomena that can occur for large times.

**2. Multiple scales.** We begin by considering (1.1) in  $t > 0$ ,  $-\infty < x < \infty$ , with appropriate Cauchy data at  $t = 0$ . Homogenisation theory can be described in several different frameworks, for example using superpositions of Bloch waves [12], but, for the moment it is simplest to use the multiple scales ansatz<sup>1</sup>

$$(2.1) \quad u \sim \sum_0^\infty \epsilon^k u_k(x, X, t),$$

with  $\frac{\partial}{\partial x}$  being replaced by  $\frac{1}{\epsilon} \frac{\partial}{\partial X} + \frac{\partial}{\partial x}$ . This idea of embedding the problem in a fictitious two-dimensional space forms the basis of the method of multiple scales [7] and it has been combined with successive rescalings of time to consider one- and two-dimensional wave propagation in [5] and [11] respectively. However for the problem we consider in the next section, more refined rescalings are necessary to produce uniformly valid asymptotic expansions that compare well with exact numerical predictions.

Since  $\frac{\partial^2 u_0}{\partial X^2}$  and  $2\frac{\partial^2 u_0}{\partial x \partial X} + \frac{\partial^2 u_1}{\partial X^2}$  are both zero, we see that if  $u_0$  and  $u_1$  are to be bounded for all  $X$  then they must be independent of  $X$ . However

$$(2.2) \quad \frac{\partial^2 u_2}{\partial X^2} - \frac{1}{c^2(X)} \frac{\partial^2 u_0}{\partial t^2} + \frac{\partial^2 u_0}{\partial x^2} = 0,$$

and we can only avoid secularity in  $u_2$  if

$$(2.3) \quad \frac{\partial^2 u_0}{\partial x^2} = \frac{1}{c_H^2} \frac{\partial^2 u_0}{\partial t^2},$$

where

$$(2.4) \quad \frac{1}{c_H^2} = \overline{\frac{1}{c^2}}$$

and the bar denotes the spatial average over a period of the function  $c$ .

The short wavelength variable  $X$  first appears in  $u_2$ , and integrating (2.2) and avoiding secular terms gives

$$(2.5) \quad \frac{\partial u_2}{\partial X} = \frac{1}{c_H^2} (I_1(X) - \bar{I}_1) \frac{\partial^2 u_0}{\partial t^2},$$

---

<sup>1</sup>If  $c$  were to depend on fast-time scale  $T = t/\epsilon$ , then  $u_k$  would also depend on  $T$ .

where

$$(2.6) \quad I_1(X) = \int^X \left( \frac{c_H^2}{c(\eta)^2} - 1 \right) d\eta$$

and

$$(2.7) \quad u_2 = \frac{1}{c_H^2} (I_2(X) - \bar{I}_2) \frac{\partial^2 u_0}{\partial t^2},$$

where

$$(2.8) \quad I_2(X) = \int^X \left( I_1(\eta) - \bar{I}_1 \right) d\eta.$$

The lower limits of the integrals are defined by the boundary conditions and are irrelevant as  $X \rightarrow \infty$ . Similarly, with a little more work, (2.3) can be shown to be the homogenisation of (1.2).

We immediately note that, in a problem in which the Cauchy data is zero in  $x > 0$ , the wavefront will approximately propagate along the leading characteristic  $x = c_M t$ , where

$$(2.9) \quad \frac{1}{c_M} = \overline{\left( \frac{1}{c} \right)}$$

and  $c_M$  is the average speed of the characteristics of (1.1) and is always greater than  $c_H$ , the homogenised wave speed<sup>2</sup>. Hence (2.3) does not describe the precursor wave field in the region of the  $(x, t)$  plane in which  $c_H < \frac{x}{t} < c_M$ . Moreover, it is also invalid in the region near  $x = c_H t$  for larger times as we now show.

We first change to variables  $\xi = x - c_H t$  and  $t$  in (1.1) to obtain

$$(2.10) \quad \frac{\partial^2 u}{\partial t^2} - 2c_H \frac{\partial^2 u}{\partial t \partial \xi} + (c_H^2 - c^2) \frac{\partial^2 u}{\partial \xi^2} = 0.$$

If we now write  $u = u(\xi, X, t)$  in a multiscale expansion, we merely retrieve (2.3) but, if we put  $t = \tau/\epsilon^2$ , as we would for the derivation of the nonlinear Schrödinger equation [9] and replace  $\frac{\partial}{\partial \xi}$  by  $\frac{\partial}{\partial \xi} + \frac{1}{\epsilon} \frac{\partial}{\partial X}$  and  $\frac{\partial}{\partial t}$  by  $\epsilon^2 \frac{\partial}{\partial \tau} + \frac{c_H}{\epsilon} \frac{\partial}{\partial X}$ , we obtain

$$(2.11) \quad \frac{\partial^2 u}{\partial X^2} + 2\epsilon \frac{\partial^2 u}{\partial \xi \partial X} - \epsilon^2 \left( \frac{c_H^2}{c^2} - 1 \right) \frac{\partial^2 u}{\partial \xi^2} + 2\epsilon^4 \frac{c_H}{c^2} \frac{\partial^2 u}{\partial \xi \partial \tau} - \frac{\epsilon^6}{c^2} \frac{\partial^2 u}{\partial \tau^2} = 0.$$

Then expanding  $u \sim U_0 + \epsilon U_1 + \dots$  shows that  $U_0$  and  $U_1$  are both independent of  $X$  but now

$$(2.12) \quad \frac{\partial^2 U_2}{\partial X^2} - \left( \frac{c_H^2}{c^2} - 1 \right) \frac{\partial^2 U_0}{\partial \xi^2} = 0.$$

Hence,

$$(2.13) \quad \frac{\partial U_2}{\partial X} = (I_1(X) - \bar{I}_1) \frac{\partial^2 U_0}{\partial \xi^2},$$

---

<sup>2</sup>As mentioned by Beryland and Burridge [2], this phenomenon was noticed in 1971 by O'Doherty and Anstey [10].

and

$$(2.14) \quad U_2 = \left( I_2(X) - \bar{I}_2 \right) \frac{\partial^2 U_0}{\partial \xi^2}.$$

A similar calculation at  $O(\epsilon^3)$  reveals that

$$(2.15) \quad \frac{\partial^2 U_3}{\partial X^2} = -2 \left( I_1(X) - \bar{I}_1 \right) \frac{\partial^3 U_0}{\partial \xi^3} + \left( \frac{c_H^2}{c^2} - 1 \right) \frac{\partial^2 U_1}{\partial \xi^2},$$

and hence that

$$(2.16) \quad \frac{\partial U_3}{\partial X} = -2 \left( I_2(X) - \bar{I}_2 \right) \frac{\partial^3 U_0}{\partial \xi^3} + \left( I_1(X) - \bar{I}_1 \right) \frac{\partial^2 U_1}{\partial \xi^2}.$$

Then the vital  $O(\epsilon^4)$  terms give

$$(2.17) \quad \begin{aligned} \frac{\partial^2 U_4}{\partial X^2} &= -2 \frac{\partial^2 U_3}{\partial X \partial \xi} + \left( \frac{c_H^2}{c^2} - 1 \right) \frac{\partial^2 U_2}{\partial \xi^2} - \frac{2c_H}{c^2} \frac{\partial^2 U_0}{\partial \xi \partial \tau} \\ &= A(X) \frac{\partial^4 U_0}{\partial \xi^4} - \frac{2c_H}{c^2} \frac{\partial^2 U_0}{\partial \xi \partial \tau} - 2 \left( I_1(X) - \bar{I}_1 \right) \frac{\partial^3 U_1}{\partial \xi^3}, \end{aligned}$$

where  $A(X) = \left( \frac{c_H^2}{c^2} + 3 \right) (I_2(X) - \bar{I}_2)$ . Finally we see that the secularity condition for  $U_4$  is

$$(2.18) \quad \bar{A} \frac{\partial^4 U_0}{\partial \xi^4} = \frac{2}{c_H} \frac{\partial^2 U_0}{\partial \xi \partial \tau},$$

which is the asymptotic limit of the dispersive Boussinesq wave equation that appears after (39) in Santosa and Symes [12] where  $\epsilon \rightarrow 0$  with  $\xi, \tau$  of  $O(1)$ . We remark that the amplitude of the rapid oscillations in  $u$  is always of  $O(\epsilon^2)$  compared to the lowest-order homogenised response.

We now consider what the above theory says about the long-time solution in a specific example.

**3. A finite-dimensional example.** One obvious situation where (1.1) can be solved analytically is when  $c$  is piecewise constant and the initial and boundary conditions are also constant. In order to focus on the effects of dispersion, we consider a case where waves would be unidirectional if the medium was homogeneous, namely

$$(3.1) \quad c^2(X) \frac{\partial^2 u}{\partial X^2} = \frac{\partial^2 u}{\partial T^2},$$

where  $T = t/\epsilon$ , with

$$(3.2) \quad u(X, 0) = \frac{\partial u}{\partial T}(X, 0) = 0, X > 0 \quad \text{and} \quad u(0, T) = 1, T > 0.$$

We take  $c$  to have period 2 for convenience and suppose

$$(3.3) \quad c = \begin{cases} 1 & : 0 < X < 1 \\ \frac{1}{2} & : 1 < X < 2 \end{cases};$$

thus  $c_H = \sqrt{0.4} \approx 0.63$  while the average characteristic speed  $c_M$  is  $\frac{2}{3}$ . This data is chosen to enable us to solve the problem exactly but unfortunately there is no initial wavelength against which to compare the lengthscale of  $c(X)$ . However, long waves will emerge as  $T \rightarrow \infty$  and, by identifying  $\epsilon^{-1}$  as a long timescale, we will be able to use homogenisation theory. The fact that  $c_M - c_H \approx 0.04$  suggests that we will have to go to times where  $T = O(10^3)$  in order to observe dispersive effects.

Our initial/boundary value problem has a discontinuity at  $X = T = 0$  which will propagate along the characteristics of the equations and will be reflected at each interface  $X = m$ , giving rise to the regular pattern shown in Figure 1. There will be non-zero discontinuities across all the characteristics in this figure except for every third reflection in the quadrilaterals adjacent to the zero initial state, but these lines are included to preserve the pattern of the ‘grid’. Away from these characteristics the solution will be piecewise constant and the grid has a repeat<sup>3</sup> in  $4m \leq X \leq 4m + 4$ ,  $2n \leq T \leq 2n + 2$  for integers  $m \geq 0$ ,  $n \geq 0$  which contains 6 cells as shown in Figure 2. We can therefore set up 6 difference equations for the constants  $a_{m,n}$ ,  $b_{m,n}$ , ...  $f_{m,n}$ , which are the values of  $u(X, T)$  in each cell. In order to obtain the relations between these quantities we need to consider the typical reflection problem shown in Figure 3, where incoming discontinuities along characteristics with velocities  $c_1$  (in  $X < 0$ ) and  $-c_2$  (in  $X > 0$ ) are incident simultaneously on the discontinuity of  $c$  at  $X = 0$ , and we need to determine the constant value  $\gamma$  of  $u$  in the region  $C = C_1 \cup C_2$  in terms of the constant values  $\alpha$ ,  $\beta$  and  $\delta$  in  $A = A_1 \cup A_2$ ,  $B$  and  $D$ . Since the solution is discontinuous, it does not obey (3.1) classically, but we can find  $\gamma$  either by considering a limit of rapidly varying smooth solutions, or by the method of weak solutions, or by using the integrated form of (3.1),

$$(3.4) \quad \frac{d}{dT} \left( \int_a^b \frac{1}{c^2} \frac{\partial u}{\partial T} dX \right) = \left[ \frac{\partial u}{\partial X} \right]_a^b,$$

which any weak solution of (3.1) must satisfy. If we take  $a < 0 < b$ , then the right-hand side is zero for times  $T$  with  $|T| < \min(|a|, b)/\max(c_1, c_2)$ , so the momentum in the interval  $(a, b)$  is constant. Evaluating  $\int_a^b \frac{1}{c^2} \frac{\partial u}{\partial T} dX$  for  $T < 0$  generates contributions from the two incoming discontinuities and is  $(\beta - \alpha)/c_1 + (\delta - \alpha)/c_2$ , whereas when  $T > 0$  it takes the value  $(\gamma - \beta)/c_1 + (\gamma - \delta)/c_2$ . Thus these two quantities are equal and we obtain

$$(3.5) \quad (\alpha + \gamma)(c_1 + c_2) = 2(\beta c_2 + \delta c_1).$$

This formula can also be obtained by the methods of [8] using the solution of an equivalent Riemann problem for the first-order form of the wave equation.

Now we can apply this formula directly at the points A,B,C,D,E,F in Figure 2 (noting that it applies equally well where  $c_1 = c_2$  at the points C and F) to obtain the equations

$$\begin{aligned} a_{m,n+1} &= \frac{4}{3}f_{m-1,n+1} + \frac{2}{3}b_{m,n+1} - a_{m,n} \\ b_{m,n+1} &= \frac{2}{3}a_{m,n} + \frac{4}{3}c_{m,n} - b_{m,n} \end{aligned}$$

---

<sup>3</sup>Such repetition occurs whenever the piecewise-constant sound speeds are rationally related, which is equivalent to the wave propagation taking place in a Goupillaud medium. Other repetitions are possible but this one is most convenient for our calculations.

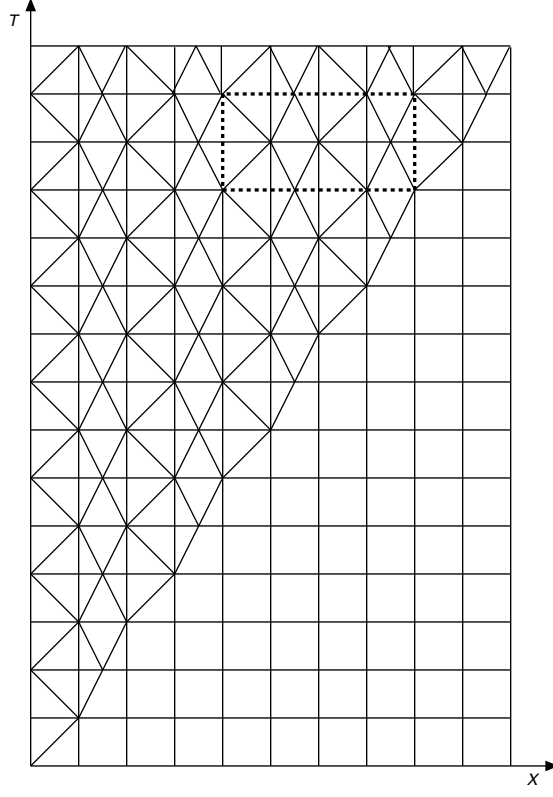


FIG. 1. Discontinuities propagating along characteristics, showing a typical element marked (see Figure 2) by the dotted rectangle.

$$\begin{aligned}
 (3.6) \quad & c_{m,n+1} = b_{m,n+1} + d_{m,n+1} - c_{m,n} \\
 & d_{m,n+1} = \frac{4}{3}c_{m,n} + \frac{2}{3}e_{m,n} - d_{m,n} \\
 & e_{m,n+1} = \frac{2}{3}d_{m,n+1} + \frac{4}{3}f_{m,n+1} - e_{m,n} \\
 & f_{m,n+1} = e_{m,n} + a_{m+1,n} - f_{m,n}.
 \end{aligned}$$

The boundary conditions mean that

$$\begin{aligned}
 a_{0,n} &= 1 & \text{for } n \geq 0, \\
 a_{m,0} &= 0 & \text{for } m \geq 1,
 \end{aligned}$$

and  $b_{m,0} = c_{m,0} = d_{m,0} = e_{m,0} = f_{m,0} = 0$  for  $m \geq 0$ . Note that these equations apply for all  $m \geq 1$  and  $n \geq 0$  although the values of  $a_{m,n}$  etc. will all be zero ahead of the positive characteristic through  $(0,0)$ .

We will give some analysis of (3.6) in section 4, but first it is very helpful to consider their numerical evaluation which is readily obtained to within rounding errors only. The solution for  $a_{m,n}$  is shown in Figures 4 and 6 at times  $T = 500$  and  $5000$  with Figure 4 corresponding to  $(x,t) = O(1)$  and  $\epsilon = 1/500$ . These figures show the main wave propagating with the homogenised wave speed  $\sqrt{0.4}$  and with a small precursor wave which is highlighted on a logarithmic scale in Figure 5. Figure 6 corresponds to

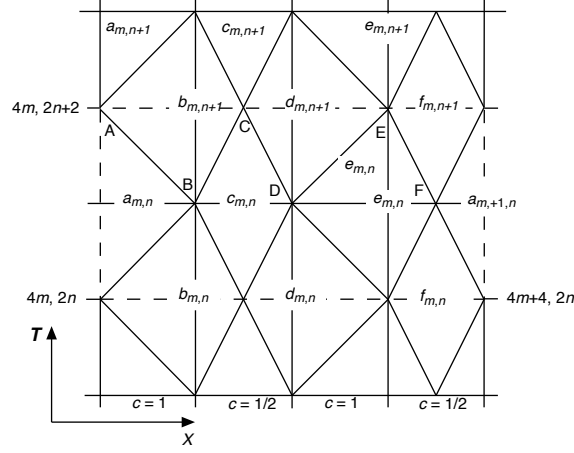


FIG. 2. Element showing the notation for the analytical solution. The region outlined by the dotted line corresponds to the typical element in Figure 1.

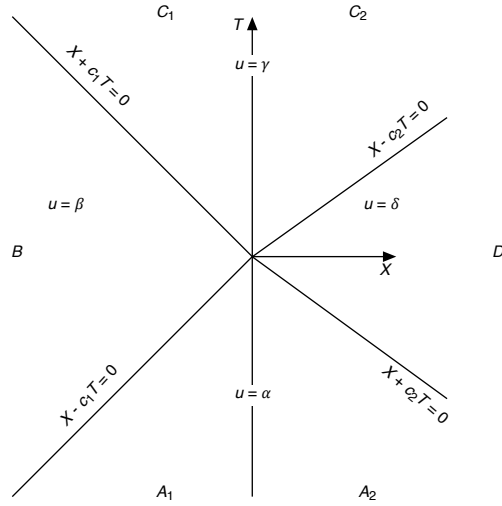


FIG. 3. Typical situation showing discontinuities along characteristics, where  $c = c_1$  in  $X < 0$ ,  $c = c_2$  in  $X > 0$ .

$x, t = O(\epsilon^{-2})$ , where, because  $\bar{A} < 0$ , the rescaled homogenised dispersive equation (2.18) can be reduced to

$$(3.7) \quad \frac{\partial^4 U_0}{\partial \xi^4} = -\sigma \frac{\partial^2 U_0}{\partial \xi \partial \tau}, \quad \sigma = \frac{100\sqrt{10}}{3},$$

with, by matching to a step function in  $\xi$  as  $\tau \downarrow 0$ ,

$$(3.8) \quad U_0(\xi, 0) = \begin{cases} 1 & \xi < 0 \\ 0 & \xi > 0 \end{cases}.$$

With  $\frac{\partial U_0}{\partial \xi} = W$  where  $W(\xi, 0) = -\delta(\xi)$ , we find from Fourier transforms that

$$(3.9) \quad W = -\left(\frac{1}{3\tau'}\right)^{1/3} \text{Ai}\left(\frac{\xi}{(3\tau')^{1/3}}\right),$$

where  $\tau' = \tau/\sigma$  and

$$(3.10) \quad \text{Ai}(x) = \frac{1}{2\pi} \int_{-\infty}^{\infty} e^{i(tx+t^3/3)} dt.$$

We will see in section 4 that the cube root of  $\tau'$  that appears in the argument of the Airy function in (3.9) is related to the fact that this solution is valid when  $T = O(\epsilon^{-3})$ . Hence

$$(3.11) \quad U_0 = \int_{\frac{\xi}{(3\tau')^{1/3}}}^{\infty} \text{Ai}(\eta) d\eta,$$

which is shown as the dashed curve in the lower graph in Figure 4. Although  $U_0$  is self-similar in  $(\xi, \tau)$ , the full solution  $u(X, T)$  is not self-similar. Also, we note that the lower graph in Figure 4 reveals an increasing discrepancy, especially in phase, between the numerical results and (3.11) as we move away from the front. This is because (3.11) is only applicable for  $x$ -variations of  $O(1)$ , and we will present an analytical representation that is more accurate in the tail of the Airy integral in Figure 10.

Precisely the same numerical evidence would have emerged had we proceeded by carrying out a “characteristic difference” calculation as described in [6] and with further detail in the book [8]. As a code validation method, the difference equations (3.6) were compared with a finite volume Godunov method as described in [8]. The finite volume method provides an exact solution when used with a unit Courant number and a Goupillaud medium such as (3.3), and was found to agree with equations (3.6) to within rounding error.

The structure of the small precursor waves in all these figures is revealed by plotting  $\log u$ , as in Figure 5 and for later times in Figure 7. This reveals an homogenised exponential decay which will shortly be shown to be an exponent having an argument proportional to  $-(X - c_H T)^{3/2}$ . The other clear feature of Figures 4 and 6 that is not revealed by homogenisation theory, is the appearance of small discrete wave packets behind the primary wave and we will now try to understand these waves by considering analytic representations of the solutions of (3.1) and (3.6).

**4. Integral Representations.** We begin by considering (3.1) for general  $c(X)$ .

**4.1. Transform Solution of (3.1).** Since  $u = 0$  in  $t < 0$ , we define the one-sided Fourier transform of  $u$  to be

$$(4.1) \quad \bar{u}(X, \omega) = \int_0^{\infty} u(X, T) e^{i\omega T} dT,$$

so that

$$(4.2) \quad u = \frac{1}{2\pi} \int_{\Gamma} \bar{u}(X, \omega) e^{-i\omega T} d\omega,$$



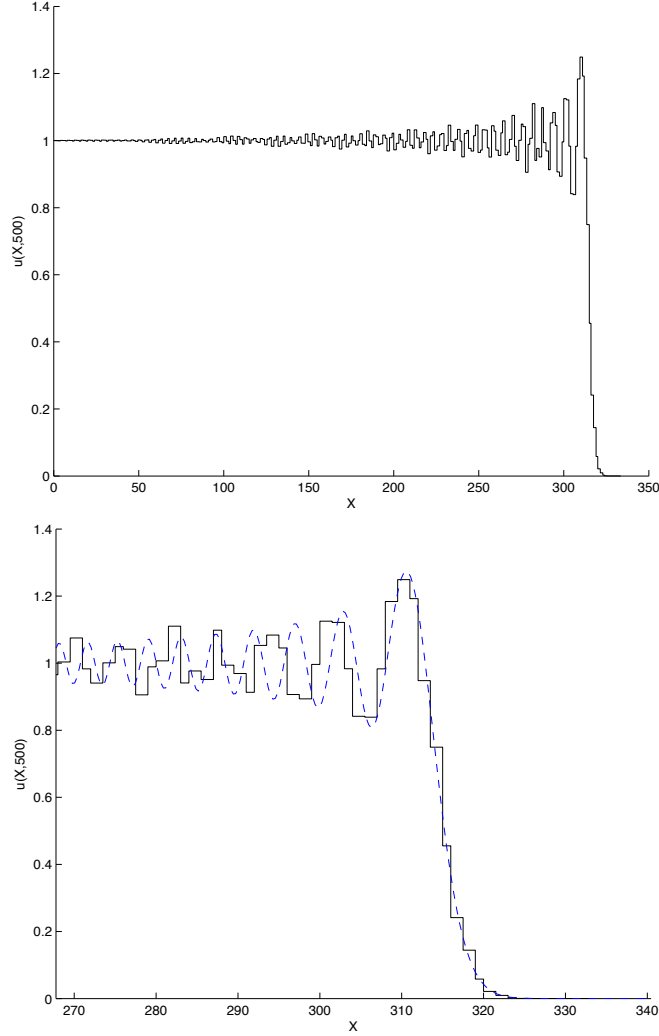


FIG. 4.  $u(X, T)$  at  $T = 500$ , with (in the lower figure) a blow-up near the front travelling at  $c_H$  and (dashed) the asymptotic form given by (3.11).

where  $\text{Im } \omega$  is assumed to be sufficiently large on the inversion contour for the integrals to converge; we will see later that it will be sufficient for  $\text{Im } \omega$  to be positive. Then (3.1) implies that

$$(4.3) \quad \frac{d^2 \bar{u}}{dX^2} + \frac{\omega^2}{c^2(X)} \bar{u} = 0$$

and we can employ Floquet theory. This shows that  $\bar{u}$  is a linear combination of functions  $F_j(X, \omega) e^{ik_j(\omega)X}$ ,  $j = 1, 2$  where  $F_j$  have the same periodicity as  $c(X)$ , which we take to be 2 henceforth. Also  $k_j$  are the roots of

$$(4.4) \quad e^{4ik} - (\bar{u}_1(2) + \frac{d\bar{u}_2}{dX}(2)) e^{2ik} + 1 = 0,$$

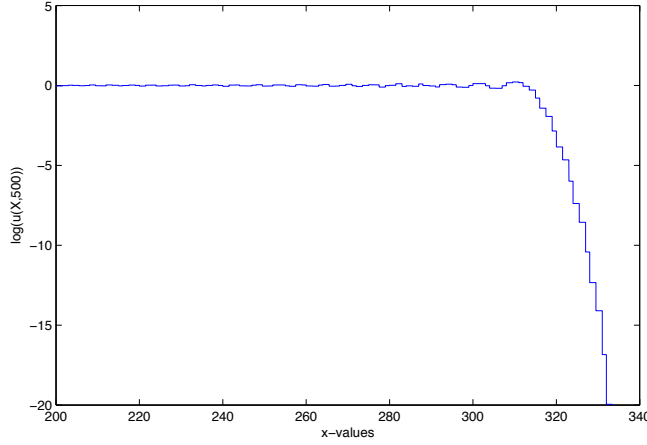


FIG. 5. The logarithm of the exact solution of the wave equation using (3.6) for 500 time steps.

where  $\bar{u}_1$  and  $\bar{u}_2$  are solutions of (4.3) satisfying

$$(4.5) \quad \bar{u}_1(0) = 1, \quad \frac{d\bar{u}_1}{dX}(0) = 0; \quad \bar{u}_2(0) = 0, \quad \frac{d\bar{u}_2}{dX}(0) = 1$$

respectively. Moreover  $F_j e^{ik_j X} = \alpha_j \bar{u}_1 + \beta_j \bar{u}_2$  where  $\begin{pmatrix} \alpha_j \\ \beta_j \end{pmatrix}$  are the eigenvectors of

$$\begin{pmatrix} \bar{u}_1(2) - e^{2ik_j} & \bar{u}_2(2) \\ \frac{d\bar{u}_1}{dX}(2) & \frac{d\bar{u}_2}{dX}(2) - e^{2ik_j} \end{pmatrix}.$$

The precise formulae for  $F_j$  are unwieldy and are recorded in the Appendix.

If  $\omega$  is real, then either

- (i)  $e^{2ik_j(\omega)}$  are both real, with product unity and  $\omega$  is said to lie in a stopband, or
- (ii)  $e^{2ik_j(\omega)}$  are complex conjugates and  $\omega$  is said to lie in a passband.

Also  $k_j(\omega)$  has branch points wherever the discriminant of (4.4) vanishes.

Although (4.3) can only be solved explicitly for a few functions  $c(X)$ , the oscillatory behaviour of  $\bar{u}$  as  $|\omega| \rightarrow \infty$  can often be revealed by the WKB expansion

$$(4.6) \quad \bar{u} \sim \text{const}(c(X))^{1/2} \exp\left(\frac{\pm i\omega}{\tilde{c}(X)}\right),$$

where

$$(4.7) \quad \frac{1}{\tilde{c}(X)} = \int_0^X \frac{d\xi}{c(\xi)}.$$

Such expansions are only valid when  $c(X)$  is continuous, in which case the passbands become thinner and thinner as  $|\omega| \rightarrow \infty$ . However in our example (3.3), this procedure is invalid and the pass and stopband structure is periodic in  $\omega$ .

**4.2. Transform Solution of (3.1, 3.2, 3.3).** In this special case, we find that, when  $k$  is real,  $k(\omega)$  has period  $\pi$  and satisfies

$$(4.8) \quad 2 \cos 2k(\omega) = 9 \cos^3 \omega - 7 \cos \omega.$$

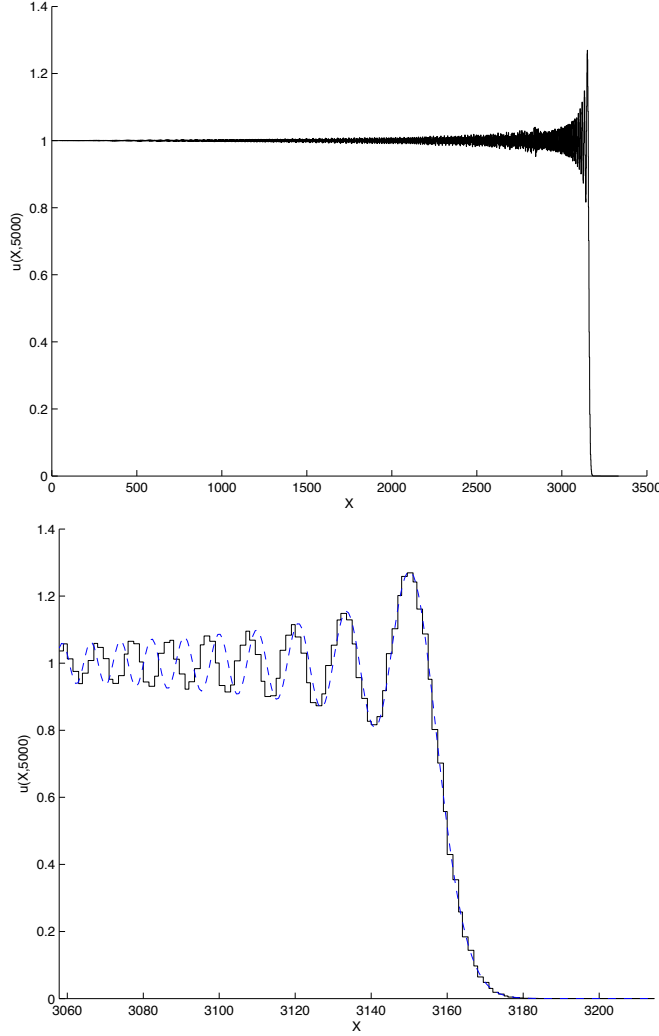


FIG. 6.  $u(X, T)$  at  $T = 5000$ , with (in the lower figure) a blow-up near the front travelling at  $c_H$  and (dashed) the asymptotic form given by (3.11).

This gives that

$$(4.9) \quad e^{2ik_j} = \chi \pm \sqrt{\chi^2 - 1},$$

where  $\chi = \frac{9}{2} \cos^3 \omega - \frac{7}{2} \cos \omega$ , which implies that  $k_j(\omega)$  has branch points when  $\chi = \pm 1$ , i.e. when

$$(4.10) \quad \cos \omega = \frac{1}{3}, \quad \frac{2}{3},$$

and for  $\frac{1}{3} < |\cos \omega(k)| < \frac{2}{3}$ ,  $k$  is purely imaginary<sup>4</sup>. The multivalued function  $\text{Re } k(\omega)$  is plotted for real  $\omega$  in Figure 8. We note that

<sup>4</sup>Although  $\chi = \pm 1$  when  $\omega = n\pi$ , these points do not require any special consideration in the asymptotic analysis since  $\omega - n\pi \sim \pm \sqrt{\frac{1}{10}}(2k - m\pi)$ , where  $m$  and  $n$  are either both odd or both even.

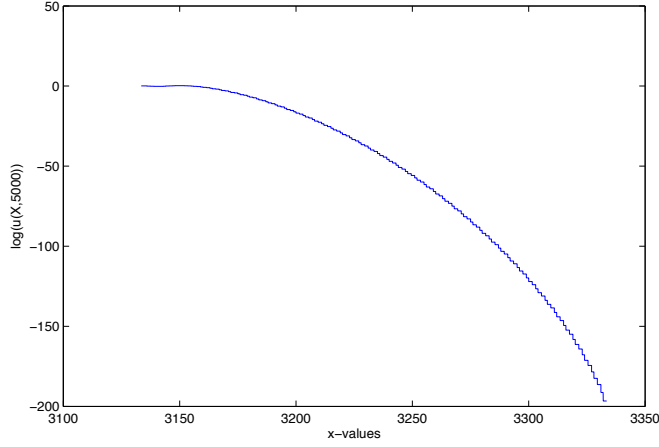


FIG. 7. Exact solution  $\log u(X, T)$  of the wave equation using (3.6) for 5000 time steps.

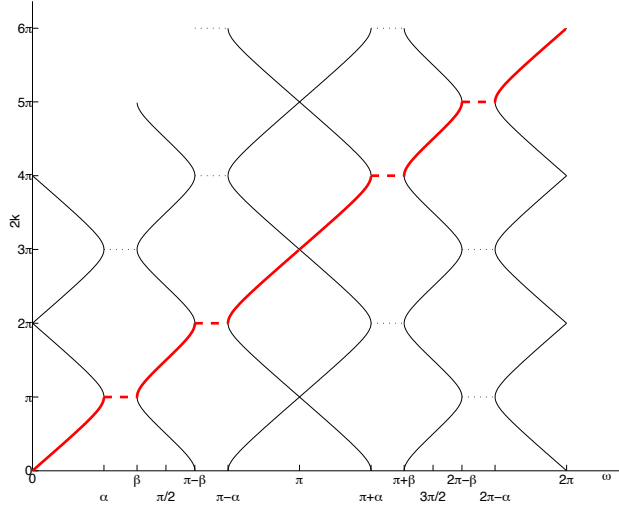


FIG. 8. Plot of  $2k(\omega)$  for real  $\omega$  with  $\cos \alpha = \frac{2}{3}$  and  $\cos \beta = \frac{1}{3}$ . The dashed lines represent  $\text{Re}(2k)$  when  $k$  is complex.

- (i) as  $|\omega| \rightarrow \infty$  with  $\text{Im } \omega > 0$ , the group velocity  $\frac{d\omega}{dk}$  is asymptotically equal to the average characteristic speed  $c_M$ ; and
- (ii) the only singularities of  $k(\omega)$  are at the ends of the pass and stopbands  $\omega = \cos^{-1} \frac{2}{3}, \cos^{-1} \frac{1}{3}, \pi - \cos^{-1} \frac{1}{3}, \pi - \cos^{-1} \frac{2}{3}$ , etc.

From our requirement that  $\text{Im } \omega > 0$  on  $\Gamma$ , the branch cuts of  $k(\omega)$  must all lie in  $\text{Im } \omega \leq 0$ .

We now have to choose the branch of  $k_j(\omega)$  so that  $u$  neither grows as  $X \rightarrow \infty$  nor contains incoming waves as  $X, T \rightarrow \infty$  with  $X < c_M T$ . This means that the branch of the square root in (4.9) must be chosen so that  $\frac{k_j(\omega)}{\omega}$  is positive in every passband,  $k_j$  being an odd function of  $\omega$  in these bands, and  $\text{Im}(k_j)$  is positive in every stopband. This can only be achieved if we choose the branch cuts and  $\Gamma$  as in

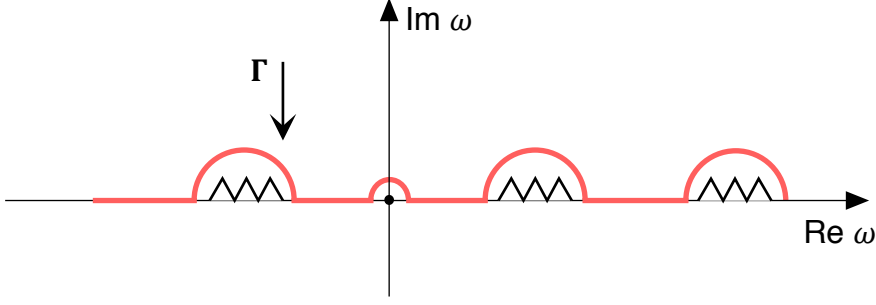
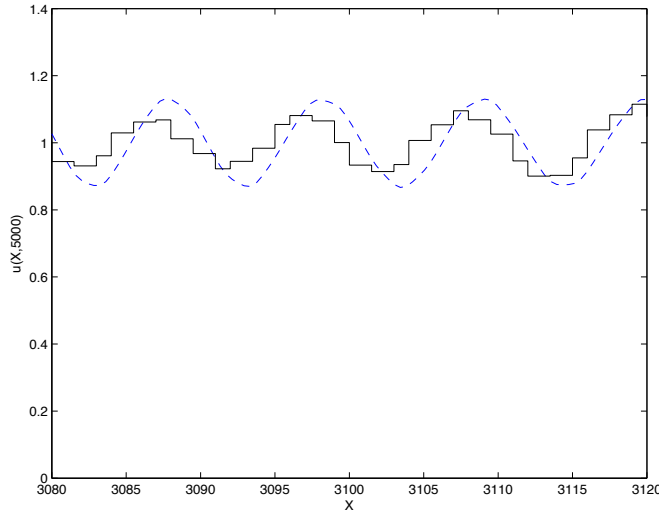
FIG. 9. The contour  $\Gamma$  showing the branch cuts.FIG. 10. Comparison of (4.14) with the numerical solution at  $T = 5000$ .

Figure 9, and then the appropriate branch of  $k_j$  is the heavy curve in Figure 8.

When we take  $F_j$  to be the corresponding 2-periodic function of  $X$  such that, without loss of generality,  $F_j(0, \omega) = 1$ , the boundary condition  $u(0, T) = 1$  implies that  $\bar{u}(0, \omega) = \frac{i}{\omega}$  and

$$(4.11) \quad u = \frac{i}{2\pi} \int_{\Gamma} e^{-i\omega T + ik(\omega)X} F(X, \omega) \frac{d\omega}{\omega},$$

where the suffix  $j$  has now been dropped. As mentioned above, when we solve (4.3), (4.5) explicitly for  $\bar{u}_1$  and  $\bar{u}_2$ , we are led to the cumbersome representation (A.1 – A.4).

For the homogeneous case  $c = \text{const}$ , the branch cuts would be absent and we could close  $\Gamma$  in the lower half plane to find the solution, which would just come from the residue at  $\omega = 0$ . The presence of the branch cuts means that the best we can do analytically is to consider (4.11) asymptotically as  $X, T \rightarrow \infty$ .

The contributions from the stopbands away from the branch points will be exponentially small as  $X \rightarrow +\infty$  and the contributions from the passbands away from the branch points will be algebraically small for large  $X, T$ . Thus, remembering that since

$F$  has period 2, the phase of any term in the Fourier representation of the integrand in (4.11) will be  $kX - \omega T + n\pi X$  where  $n$  is an integer, the leading-order wave perceived by an observer moving with speed  $V$  will come from values of  $\omega$  such that the phase is stationary. i.e.,

$$(4.12) \quad \frac{d}{d\omega}(Vk(\omega)) = 1.$$

Writing the inverse of the group velocity as

$$(4.13) \quad \frac{1}{V} = \frac{dk}{d\omega}(\omega_V),$$

the local waveform for most values of  $V$  will be proportional to a sum over integer  $n$  of terms of the form

$$(4.14) \quad \frac{F(X, \omega_V)}{\omega_V} \times \exp[-i\omega_V T + i(VT + \zeta)(k(\omega_V) + n\pi)] \times \\ \times \int_{-\infty}^{\infty} \exp\left[i\zeta(\omega - \omega_V)k'(\omega_V) + \frac{i}{2}VTk''(\omega_V)(\omega - \omega_V)^2\right] d\omega,$$

where  $X - VT = \zeta$ , and the main contribution to the integral comes from  $\omega - \omega_V = O(\zeta/T)$  as  $T \rightarrow \infty$  with  $1 \ll \zeta \ll T$ . Remembering that  $k'(\omega_V) = \frac{1}{V}$  and writing

$$(4.15) \quad \omega - \omega_V = \eta \sqrt{\frac{2}{VT|k''(\omega_V)|}},$$

we see that each term is a harmonic wave modulated by

$$(4.16) \quad \frac{(1+i)\sqrt{\pi}}{\sqrt{VT|k''(\omega_V)|}} \exp\left[-i\frac{\zeta^2}{2V^3T|k''(\omega_V)|}\right],$$

which is of  $O(T^{-1/2})$  as  $T \rightarrow \infty$ . As expected from our discussion at the end of Section (3), (4.14), with the integral given by (4.16), provides a good approximation to the numerical prediction in Figure 6 as evinced by Figure 10 which shows solution (4.14) with a value of  $\omega_V$  corresponding to  $x = 3100$ .

However this asymptotic behaviour no longer occurs where  $k''(\omega_V)$  vanishes, which happens in the centre of each passband and in particular at  $\omega = 0$  (see Figure 8). For  $\omega \neq 0$ , when we repeat the manipulations described above and we find that  $u$  is a plane wave modulated by

$$(4.17) \quad \int_{-\infty}^{\infty} \exp\left[i\zeta\frac{(\omega - \omega_V)}{V} + \frac{i}{6}k'''(\omega_V)(\omega - \omega_V)^3VT\right] d\omega$$

as  $T \rightarrow \infty$ . With

$$(4.18) \quad \omega - \omega_V = \eta \frac{2^{1/3}}{(k'''(\omega_V)VT)^{1/3}},$$

where the real cube root is chosen to avoid exponential growth as  $\zeta \rightarrow \infty$ , this becomes

$$(4.19) \quad \left(\frac{2}{VTk'''(\omega_V)}\right)^{1/3} \int_{-\infty}^{\infty} \exp i\left[\frac{\eta^3}{3} + \frac{2^{1/3}\zeta\eta}{(V^4Tk'''(\omega_V))^{1/3}}\right] d\eta,$$

the integral being  $2\pi\text{Ai}\left(\frac{2^{1/3}\zeta}{(V^4T k'''(\omega_V))^{1/3}}\right)$ . As shown in Figures 4 and 6, this Airy function modulation accurately describes the secondary wave packets.

This analysis no longer applies near  $\omega = 0$ , where the saddle-point contribution combines with the contribution from the pole. This means that the integral in (4.19) is multiplied by  $\frac{1}{\eta}$  and the contour  $\Gamma$  lying above the pole is as shown locally in Figure 9.

More precisely we have, with  $Vk'(0) = 1$ ,  $2k(\omega) \sim \sqrt{10}\omega + \frac{3\omega^3}{8\sqrt{10}} + \dots$  as  $\omega \rightarrow 0$ . So this gives  $V = \sqrt{\frac{2}{5}} = c_H$ , the homogenised wave speed. Then the major contribution to the integral comes from

$$(4.20) \quad \int_{\Gamma} \exp \left[ i \left( \frac{\eta^3}{3} + \left( \frac{80}{9T} \right)^{1/3} \frac{\zeta\eta}{V} \right) \right] \frac{d\eta}{\eta},$$

which is now proportional to the integral of the Airy function

$$(4.21) \quad \text{Ai} \left[ \left( \frac{80}{9T} \right)^{1/3} \left( \sqrt{\frac{5}{2}} X - T \right) \right],$$

as in Figure 4. Note that expression (4.21) is identical with (3.9) after the crucial substitution  $T = \epsilon^{-3}\tau$ . This result also reveals the interesting fact that (4.21) is not only valid near the primary wave where

$$(X - c_H T)/T^{1/3} = O(1)$$

but also that its exponentially small precursor is of

$$O \left( \exp \left[ -\frac{2}{3} \sqrt{\frac{80}{9T}} \left( \sqrt{\frac{5}{2}} X - T \right)^{3/2} \right] \right)$$

in the region between the primary wave and the leading wavefront  $X = c_M T$ ; this is in accordance with the predictions in Figures 5 and 7.

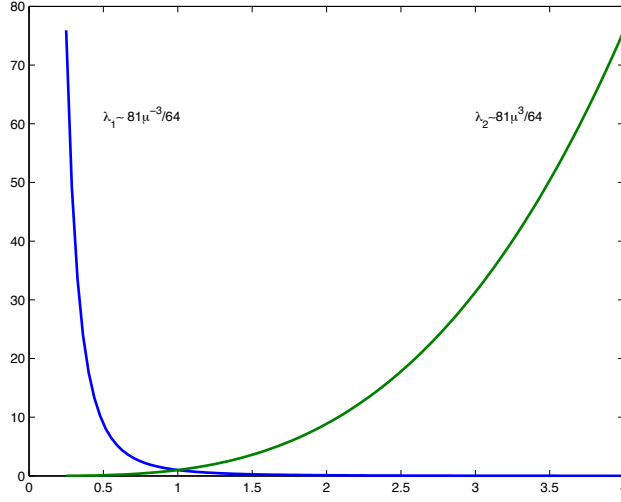
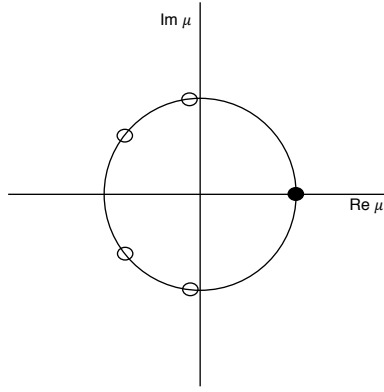
**4.3. Superposition of Power-Law Solutions of (3.6).** Equations (3.6) have solutions in which  $a_{m,n}$  is proportional to  $\lambda^m \mu^n$  as long as  $\lambda$  satisfies the quadratic equation

$$\det \begin{pmatrix} \lambda(\mu+1) & -\frac{2}{3}\mu\lambda & 0 & 0 & 0 & -\frac{4}{3}\mu \\ -\frac{2}{3} & (1+\mu) & -\frac{4}{3} & 0 & 0 & 0 \\ 0 & -\mu & (1+\mu) & -\mu & 0 & 0 \\ 0 & 0 & -\frac{4}{3} & (1+\mu) & -\frac{2}{3} & 0 \\ 0 & 0 & 0 & -\frac{2}{3}\mu & (1+\mu) & -\frac{4}{3}\mu \\ -\lambda & 0 & 0 & 0 & -1 & (1+\mu) \end{pmatrix} = 0.$$

This gives

$$(4.22) \quad \lambda^2 - 2S(\mu)\lambda + 1 = 0$$

where  $\mu^3 S$  is a sextic polynomial in  $\mu$  and we denote the roots by  $\lambda_{1,2}(\mu) = S \pm \sqrt{S^2 - 1}$ . When we identify  $2n$  with  $T$  and  $4m$  with  $X$ , we can see that this equation is analogous to (4.4), with  $\lambda = e^{2ik}$ . Also, when  $\mu$  is real, the real roots of (4.22) are as shown in Figure 11.

FIG. 11. Solutions  $\lambda$  of (4.22) for real  $\mu$ .FIG. 12. Singularities of  $A_1(\mu)(\lambda_1(\mu))^m$ . There are branch points which lie at  $\text{Re } \mu = -1/9, -7/9$  on the unit circle and a pole at  $\mu = 1$ .

Superposition now gives that

$$(4.23) \quad a_{m,n} = \int_{C_1} A_1(\mu)(\lambda_1(\mu))^m \mu^n d\mu + \int_{C_2} A_2(\mu)(\lambda_2(\mu))^m \mu^n d\mu,$$

where  $C_i$  are suitably chosen contours in the complex- $\mu$  plane. When  $m = 0$ , we require that

$$(4.24) \quad 1 = \int_{C_1} A_1(\mu) \mu^n d\mu + \int_{C_2} A_2(\mu) \mu^n d\mu \quad \text{for } n \geq 0$$

and, when  $n = 0$ ,

$$(4.25) \quad 0 = \int_{C_1} A_1(\mu)(\lambda_1(\mu))^m d\mu + \int_{C_2} A_2(\mu)(\lambda_2(\mu))^m d\mu \quad \text{for } m \geq 1.$$



This derivation could be made more systematic using operational calculus as described in [13]; this would involve writing the transform

$$(4.26) \quad \bar{a}(p, q) = \sum_{m, n=0}^{\infty} a_{m, n} e^{-pm - qn}$$

in (3.6), where  $\lambda = e^p$ ,  $\mu = e^q$ . Using the operational calculus result that if

$$\bar{a}(p) = \sum_{m=0}^{\infty} a_m e^{-pm},$$

then

$$a_m = \frac{1}{2\pi i} \int_0^{2\pi i} \bar{a}(p) e^{pm} dp,$$

which is the formal analytic continuation of the theory of Fourier series, we find that

$$a_{m, n} = -\frac{1}{4\pi^2} \oint \oint \bar{a}(\log \lambda, \log \mu) \lambda^{m-1} \mu^{n-1} d\lambda d\mu;$$

the inversion contours are  $|\lambda| = 1 + 0$ ,  $|\mu| = 1 + 0$ , which ensures that  $\text{Re } p, q > 0$ , and hence convergence of the series for  $\bar{a}$ .

When the appropriate summations are made in (3.6), we find that  $\bar{a}$  has poles on the unit circle in the  $\lambda$ -plane only at  $\lambda = \lambda_1(\mu)$  and  $\lambda_2(\mu)$ , leading to the representation in (4.23). Hence we can take  $C_1$  and  $C_2$  to be  $|\mu| = 1 + 0$  and moreover, since the integrands are holomorphic in  $|\mu| > 1$  we can let both contours become large circles.

Noting that  $\lambda_1 \sim \frac{64}{81\mu^3}$  and  $\lambda_2 \sim \frac{81\mu^3}{64}$  as  $|\mu| \rightarrow \infty$ , then<sup>5</sup>, for large  $m, n$ , the first integral in (4.23) will be zero for  $n < 3m$  and hence represents a wave travelling to the right with speed  $c_M$ . Similarly the second integral represents a wave travelling to the left with speed  $c_M$  and so we must take  $A_2(\mu) = 0$ . Finally to satisfy (4.24) and (4.25) we take

$$A_1(\mu) = \frac{1}{2\pi i(\mu - 1)}.$$

Since (4.22) tells us that  $\lambda_1$  has a triple pole at  $\mu = 0$  and 4 branch points on the unit circle as in Figure 12, we can take  $C_1$  to be any closed curve containing all these singularities, with the branch cuts all lying inside  $|\mu| = 1$  (which is possible since they are in conjugate pairs). Having ensured that  $a_{m, n} = 0$  when  $n < 3m$ , we now note for  $n \geq 3m$  the presence of the exponential  $\exp(m \log \lambda_1(\mu) + n \log \mu)$  in (4.23) implies that there is a saddle point whenever

$$\frac{m}{n} = -\frac{\lambda_1(\mu)}{\mu \lambda_1'(\mu)}.$$

This means that a saddle point approaches the pole at  $\mu = 1$  as  $\frac{m}{n} \rightarrow \frac{1}{\sqrt{10}}$  (or  $\frac{X}{T} \rightarrow \sqrt{0.4}$ ), leading to the asymptotic behaviour encountered in (4.11). This in turn

---

<sup>5</sup>Remember that  $X = 4m$ ,  $T = 2n$  as in Figure 2.

means that our representation

$$(4.27) \quad a_{m,n} = \int_{|\mu|=\text{const}>1} A_1(\mu) (\lambda_1(\mu))^m \mu^n d\mu$$

predicts that secondary wave packets will emerge from the saddle-point contributions to the integral, each of which can be identified with the contribution to (4.11) from a segment of length  $2\pi$  in the inversion contour  $\Gamma$  (Figure 9).

**5. Discussion and Conclusion.** For the model (3.1), (3.3), both the exact analytical representation of the solution (4.11) and the numerical solution, which is exact to within rounding errors, predict large time dispersive behaviour typified by Figures 4 – 7. The results reveal that the homogenised equation (2.18) predicts the waveforms more and more accurately as time increases. Indeed, not only does the dominant leading wave travel at speed  $c_H$  and disperse according to the solution of (2.18) that is the integral of an Airy function, but the exponentially small precursor to this wave which lies in  $c_H T < X < c_M T$  is accurately described by the asymptotic expansion of this integral. However, a trail of secondary dispersive wave packets follow this leading wave each of which is described by an Airy function that decays algebraically in time. Everywhere, variations on the  $X, T$  scales are small corrections to the homogenised wave profile.

It would be interesting to know if such trains of wave packets occur for more general  $c(X)$ , particularly smooth functions for which WKB expansions (4.6) could be used, and for more general initial/boundary conditions. If a similar scenario does evolve, the results of section 4 suggest that the packets travel at the group velocity  $\frac{d\omega}{dk}$  where  $\omega''(k) = 0$  and that a primary wave occurs when both  $\omega$  and  $\omega''$  vanish. Of greatest interest for the future is the use of systematic multiscaling for wave propagation in higher dimensions following from the interesting results of [11].

**Appendix.** For reference we record that, in the notation of (4.4) (4.5),

$$(A.1) \quad \bar{u}_1 = \begin{cases} \cos \omega X & : 0 < X < 1 \\ (\cos \omega \cos 2\omega + \frac{1}{2} \sin \omega \sin 2\omega) \cos 2\omega X + \\ (\cos \omega \sin 2\omega - \frac{1}{2} \sin \omega \cos 2\omega) \sin 2\omega X & : 1 < X < 2 \end{cases}$$

$$(A.2) \quad \omega \bar{u}_2 = \begin{cases} \sin \omega X & : 0 < X < 1 \\ (\sin \omega \cos 2\omega - \frac{1}{2} \cos \omega \sin 2\omega) \cos 2\omega X + \\ (\sin \omega \sin 2\omega + \frac{1}{2} \cos \omega \cos 2\omega) \sin 2\omega X & : 1 < X < 2 \end{cases}$$

so that  $\bar{u}_1(2) = 3 \cos^3 \omega - 2 \cos \omega$ ,  $\bar{u}_1'(2) = \omega \sin \omega (1 - 6 \cos^2 \omega)$ ,  $\bar{u}_2(2) = (2 \sin \omega - 3 \sin^3 \omega)/\omega$  and  $\bar{u}_2'(2) = 6 \cos^3 \omega - 5 \cos \omega$ . When  $F_j(0, \omega) = 1$ , this means that

$$(A.3) \quad F_j(X, \omega) e^{ik_j X} = \bar{u}_1 + \beta_j \bar{u}_2$$

where

$$(A.4) \quad \beta_j = \frac{(e^{2ik_j} - 3 \cos^3 \omega + 2 \cos \omega) \omega}{2 \sin \omega - 3 \sin^3 \omega},$$

and  $e^{ik_j}$  satisfies (4.4).

**Acknowledgements** The authors are grateful to Marcus Grote and Christian Stohrer who first brought this problem to their attention.

## REFERENCES

- [1] A. ABDULLE, M.J. GROTE, AND C. STÖHRER, *Finite element heterogeneous multiscale method for the wave equation: Long-time effects*. Multiscale Model. Simul. Vol. 12, No 3, pp. 1230-1257, 2014.
- [2] L. BERYLAND, AND R. BURRIDGE, *The accuracy of the O'Doherty-Anstey approximation for wave propagation in highly disordered stratified media*. Wave Motion Vol. 21, pp. 357-373, 1995.
- [3] R. BURRIDGE, G.S. PAPANICOLAOU, AND B.S. WHITE, *One-dimensional wave propagation in a highly discontinuous medium*. Wave Motion Vol. 10, pp. 19-44, 1988.
- [4] T. DOHNAL, A. LAMACZ, AND B. SCHWEIZER, *Bloch-wave homogenization on large time scales and dispersive effective wave equations*. Multiscale Model. Simul. Vol. 12, No 2, pp. 488-513, 2014.
- [5] J. FISH, AND W. CHEN, *Uniformly valid multiple-temporal scale modeling for wave propagation in heterogeneous media*. Mechanics of Composite Materials and Structures, Vol. 8, pp. 81-99, 2001.
- [6] T.R. FOGARTY, AND R.J. LEVEQUE, *High-resolution finite-volume methods for acoustic waves in periodic and random media*. J. Acoust. Soc. Am. Vol. 106, No 1, pp. 17-28, July 1999.
- [7] J. KEVORKIAN, AND J.D. COLE, *Multiple Scale and Singular Perturbation Methods*. Springer, New York, 1996.
- [8] R.J. LEVEQUE, *Finite Volume Methods for Hyperbolic Problems*. Cambridge University Press, 2002.
- [9] H. OCKENDON, AND J.R. OCKENDON, *Waves and Compressible Flow* (New York: Springer-Verlag) 2010.
- [10] R.F. O'DOHERTY, AND N.A. ANSTEY, *Reflections on amplitudes*. Geophys. Prospect. Vol. 19, pp. 430-458, 1971.
- [11] M. QUEZADA DE LUNA, AND D.I. KETCHESON, *Two-dimensional wave propagation in layered periodic media*. SIAM J. Appl. Math. Vol. 74, No 6, pp. 1852-1869, 2014.
- [12] F. SANTOSA, AND W.W. SYMES, *A dispersive effective medium for wave propagation in periodic composites*. SIAM J. Appl. Math. Vol. 51, No 4, pp. 984-1005, August 1991.
- [13] B. VAN DER POL, AND H. BREMMER, *Operational Calculus* (Cambridge University Press) 1950.
- [14] D.H. YONG, AND J. KEVORKIAN, *Solving boundary-value problems for systems of hyperbolic conservation laws with rapidly varying coefficients*. Stud. Appl. Math. Vol. 108, No 3, pp. 259-303, April 2002.